Geothermal Energy

Preliminary fluid geochemical survey in Tete Province and prospective development of geothermics in Mozambique

M. Procesi[1*] , L. Marini[2], D. Cinti[1], A. Sciarra[1], P. Basile[2], T. Mazzoni[2] and F. Zarlenga[3]

*Correspondence:
monia.procesi@ingv.it
[1] Istituto Nazionale Di
Geofisica e Vulcanologia,
Rome, Italy
Full list of author information
is available at the end of the
article

Abstract

An evaluation of the feasible development of geothermal energy in Mozambique is proposed based on some thermal springs geochemical characterization in the Tete region. Chemical and isotopic data suggest that the springs have a meteoric origin and do not show connection with any active magmatic system. The proposed circulation model suggests high depths infiltration of meteoric waters along faults and fractures in a system characterised by discrete permeability and reservoir temperature between 90 and 120 °C. These results, jointly with low salinity fluids and corrosive components absence suggest that the geothermal system may be conveniently exploited for direct and indirect uses.

Keywords: Fluid geochemistry, Geothermometry, Geothermal energy, Mozambique, Tete

Introduction

Mozambique is located on the southwestern branch of the East African Rift System (EARS) and borders on Malawi, Zambia, Tanzania, Zimbabwe, South Africa and Swaziland. The total area is about 800,000 km^2 and divides into 11 provinces. After a long period of colonial rule by Portugal, ended in 1975, Mozambique is, at present, an independent republic. Its economy is mainly based on agriculture (Chambal 2010), it is rich in a variety of natural resources, such as forests, marine resources, minerals and hydro-resources, but it suffers from extremely low access to energy and scarce sustainable utilization. This situation is partly due to the fact that most of the produced energy is transported to other countries (especially South Africa), to the lack of power transmission lines and distribution networks, to the high cost of extending networks; and finally to the high use of conventional fuels (e.g., gasoline) especially in remote and relatively low demand areas. In fact, electricity in rural areas is largely supplied by diesel generators and at present, as a matter of fact, only 29% of the population has access to electricity and it is mainly restricted to urban areas. Therefore, new energy solutions should be thought of, considering and adapting to the reality of the Country and by combining

the intensification of electrification by the national electricity grid with the adoption of available and sustainable renewable energy sources of which the Country is rich.

The potential renewable energy resources in Mozambique are highlighted in Fig. 1, whereas the relative energy potential for each resource is shown in Table 1. Unfortunately, at the present, renewable resources in Mozambique are confined, for about 90% (Chambal 2010), to traditional biomass uses (i.e., wood for cooking) and rarely to off-grid power supply source, such as solar, hydro, modern biomass fuels, wind and geothermics.
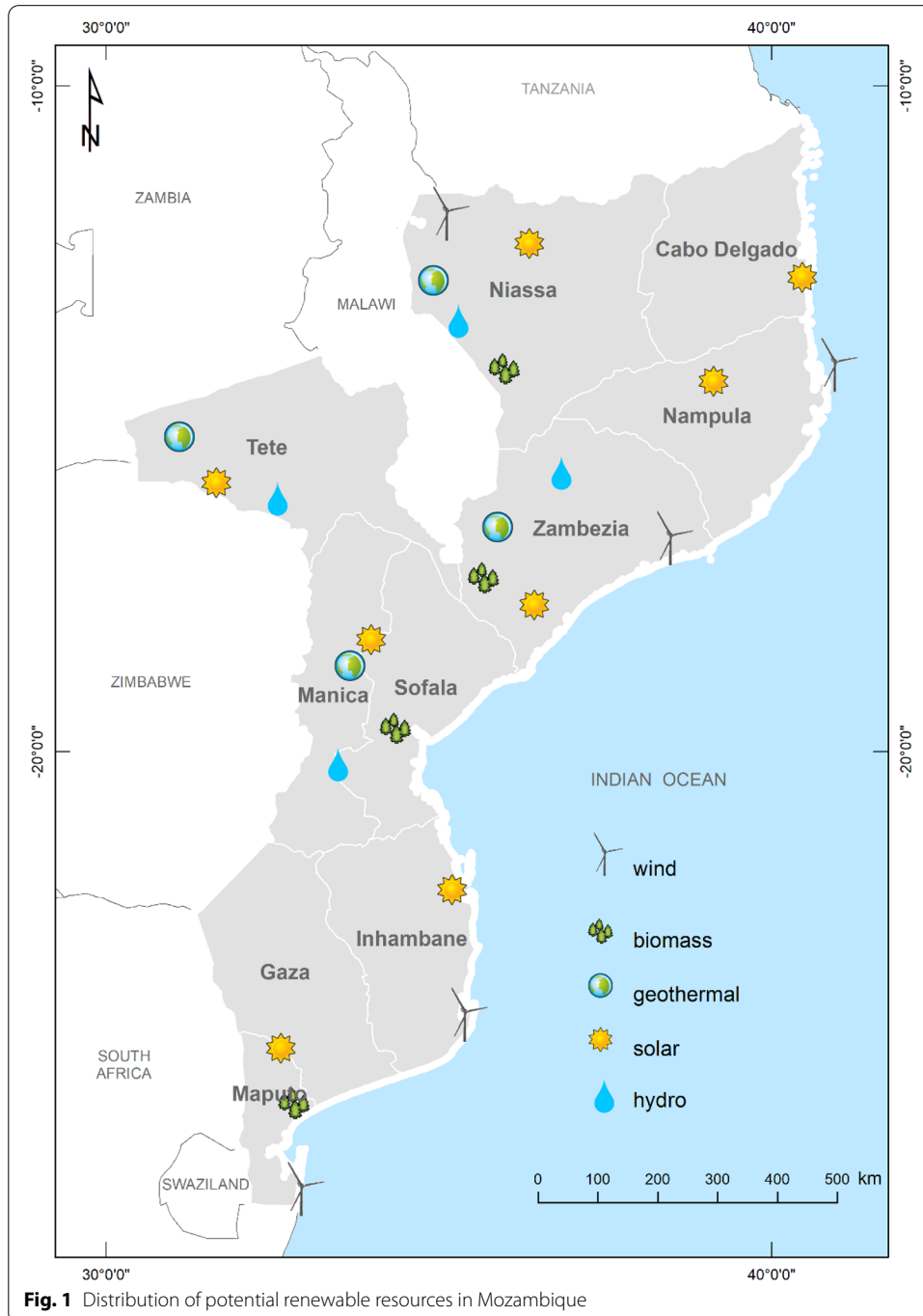

Fig. 1 Distribution of potential renewable resources in Mozambique

Procesi *et al. Geothermal Energy*   (2022) 10:2

Page 3 of 27

Table 1 Typology of renewable resources in Mozambique, location and estimated energy potential (from IRENA 2012; Gesto 2014; Mokveld and Von Eije 2018.)

Resources	Sites	Energy potential
Hydro	Zambezi Valley & other sites	19 GW (small Hydro > 1000 MW)
Biomass	Countrywide	2GW
Solar	Countrywide	23TW
Wind	Coast & Niassa Provinces	4.5 GW Speed 7 m/s (> 7 m/s in some areas)
Geothermal	Tete, Niassa, Manica & Zambezia Provinces	147 MW

Currently, the Cahora Bassa hydropower plat is the main source of power generation in the country and represents one of the largest dams in Africa. Despite this, solar is the primary renewable resource of Mozambique with a potential of 23 TW, followed by hydro, wind, biomass and geothermics, but all these resources are poorly employed.

The development of geothermal energy, in both direct and indirect uses, could represent an important goal for the improvement of the energy distribution and network in the Country and for the economic growth, especially considering the Provinces closest to the southwestern branch of the East African Rift System (EARS), where several thermal springs are present. In addition, considering the modern geothermal technologies, also in areas, where the geothermal gradient is not so high, the utilization of unconventional Geothermal System (i.e., Enhanced Geothermal System, EGS) could be an important solution to consider. Moreover, the geothermal energy shares many of the advantages of most other renewables resources. In particular, it is always available, 24 h a day and 365 days a year, and it does not depend on season and weather conditions, such as solar and wind power. Moreover, geothermal energy does not require large spaces, it is a silent energy, both power and domestic plants have long average life spans (more than 50 years) and do not require special maintenance. In light of this and as mentioned before, Mozambique is rich in thermal springs, especially in the northern and central parts, with temperatures that can reach 95 °C. Despite these interesting features and the proximity with the East African Rift System, the geothermal exploration of the Country is unfortunately still at an embryonic state. Few preliminary studies were conducted between the end of the seventies and eighties, but only in the last years, the interest in the geothermal potential of Mozambique has deeply revived. As a consequence, the pertinent scientific literature is still extremely limited and this fact represents a serious obstacle for the geothermal development in the Country. The first estimates of the geothermal potential of Mozambique were made by Mc Nitt (1978, 1982), who indicated the northern and the central provinces of the Country as the most promising areas. Other preliminary reports were performed by BRGM (1980), Aquater (1980) and Direcçao Nacional de Geologia (1981). The preliminary results were confirmed years later by Martinelli et al. (1995) and, more recently, by Gesto Energia (2014) and Procesi et al. (2015). In particular, the Renewable Energy Atlas of Mozambique (Gesto Energia 2014), commissioned in 2013 by the Government of Mozambique, reported the preliminary conclusions of the geothermal survey carried out on six provinces of the Country (Manica, Tete, Nampula, Niassa, Zambézia and Sofala). In four sites (Boroma, Namacurra, Morrumbala and Maganja da Costa in Zambézia Province) reservoir temperatures between

Procesi *et al. Geothermal Energy* (2022) 10:2

Page 4 of 27

150 and 164 °C have been estimated. Moreover, for six selected sites in the provinces of Tete, Zambézia and Niassa, a potential geothermal reservoir depth between 1500 and 2500 m has been estimated by magnetotelluric and gravity surveys and a geothermal potential of 147 MW has been predicted. The existence and the characteristics of these potential reservoirs could only be confirmed through a drilling program but the medium-range estimated reservoir temperatures (~ 150 °C) give back high project costs and potentially high mining risk. Beyond that, the most enigmatic prospect remains probably the Metangula area, where hot springs with outlet temperature > 95 °C (the highest of the whole country) were reported to be present on the lake Niassa-Malawi shores before the rise in the lake water level (Martinelli et al. 1995 and references therein) but chemical data are not available. In spite of the favourable geological framework and although the National Government of Mozambique has financed preliminary feasibility studies, at present there is only one exploration project in the whole Country and no active geothermal power plants. The issue could be related to the fact that the geothermal interest and exploration in Africa is relatively recent and especially focused on high-temperature systems. Moreover, since decades, the entire African territory and Mozambique also, are deeply explored for hydrocarbon exploitations, especially by foreign Countries, and the renewable resources have been so far poorly considered. Fortunately, as mentioned before, the African National Governments, such as Mozambique, are now taking interest in renewable and sustainable resources as geothermics. In sigh of this, here we propose an in-depth analysis of the study partly presented in Procesi et al. (2015) through an overview on available data about thermal waters in Mozambique with the presentation of new collected data in the Tete Province (Northwestern Mozambique). The aims of the study are: (1) to estimate the temperature of the potential geothermal reservoir(s); (2) to propose a conceptual circulation model constrained by the chemical–physical conditions of thermal waters and the geological, structural and hydrogeological framework, and in this way (3) provide a useful reference for the further national strategic energy planning.

Geological, structural and hydrogeochemical setting of Tete Province

The territory of Mozambique is part of three major lithospheric plates (East, West and South Gondwana) that collided during the Pan African orogenic cycle (800–550 million years). West and South Gondwana are divided by an important shear zone: the Sanangoè Shear zone (SSZ). All of these major plates are present in the Tete Province (Western Mozambique). The most recent tectonic cycle of Mozambique is relative to the Post-Gondwana Cycle. It began 175 million years ago and consisted of the final break-up of the Gondwana continent, followed by a phase of epeirogenesis and several neo-rifting phases. The rifting processes created lowlands covered by Karoo and post-Karoo Formations, and highlands and mountains constituted by Precambrian crystalline basement rocks (Steinbruch et al. 2008). Despite the paucity of detailed geological, hydrogeological and structural information on the Mozambican territory, the recent mapping, at the scale 1:250.000, of most of the country made by the GTK Consortium (Pekkala et al. 2008) provided an overview on the geological–structural and hydrogeological setting of the Tete Province.

From the structural point of view, the Tete Province is dominated by the Zambezi rift, which trends W–E from the Zambia/Zimbabwe border along Cahora Bassa and swings SE towards Tete and onwards to the coast of Mozambique (Hatton and Fardell 2021) (Fig. 2A, B). The rift affected the Precambrian basement rocks and developed into a zone of active extensional tectonism with sedimentary deposition. In the study area, two main stratigraphic units are recognized, from top to bottom: the Karoo Supergroup (Carboniferous–Cretaceous) and the Pre-Karoo Formations of the Precambrian Basement (Hatton and Fardell 2021) (Fig. 2B, C). The Karoo Supergroup overlies the basement rocks with a significant unconformity and comprises detrital sedimentary lithotypes and coal-bearing horizons, intruded at a late stage by doleritic dykes and sills. The rocks of the Karoo Supergroup outcropping in the study area are those of the lower Karoo (Dwyka Stage—Ecca Group; Carboniferous–Early Permian), consisting of tillite, fluvio-glacial deposits and thick sandy–argillaceous deposits with interstratified coal seams (Fig. 2C). The Precambrian basement comprises rocks of the Tete Suite and of the Southern Crystalline Basement. The latter, exposed south of the Sanangoè Shear Zone (SSZ) (Westerhof et al. 2008a) is mainly composed by the Chìdué Group and Chacocoma Granite (Westerhof et al. 2008b) (Fig. 2B, C). The Chìdué Group is mainly constituted by gneisses, marbles and meta-sandstones. These rocks were modified by contact-parallel tectonic below the Tete Suite. The Chacocoma Granite is highly deformed and the original porphyritic rock is obscured by Augen gneiss texture. Close to the tectonic contact with the Tete Suite, the granitoid was deformed into (blasto)mylonites and phyllonites (Westerhof et al. 2008b). The Tete Suite is a layered intrusive, composed predominantly of gabbro, with subordinate leucogabbro, norite, anorthosite and pyroxenite. Lenses of
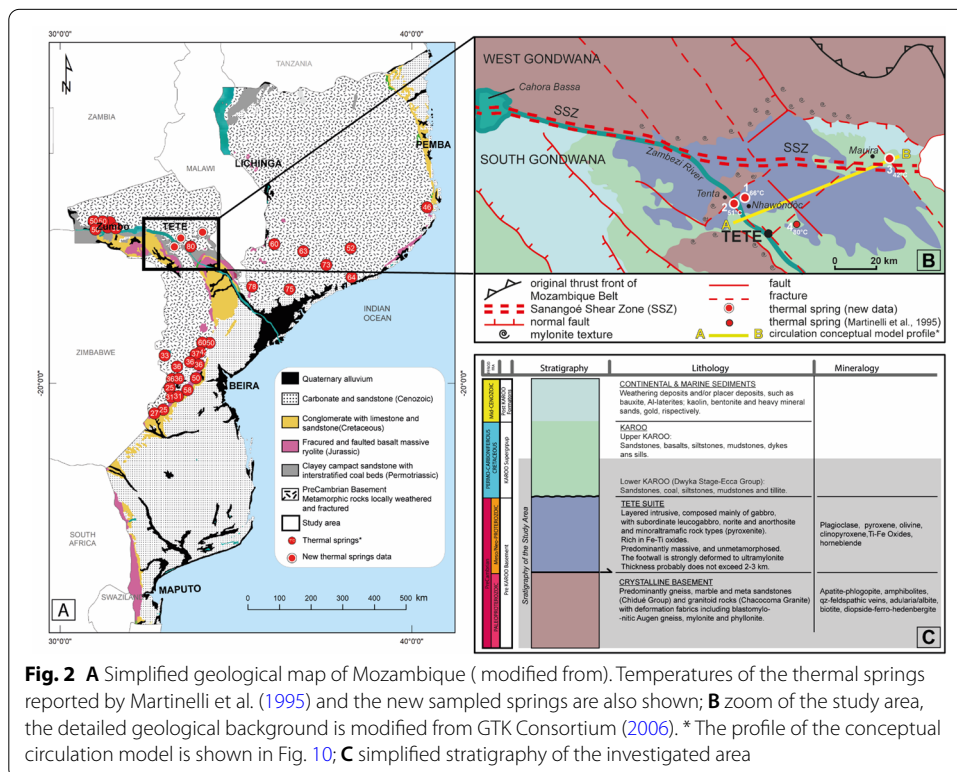

Fig. 2 A Simplified geological map of Mozambique (modified from). Temperatures of the thermal springs reported by Martinelli et al. (1995) and the new sampled springs are also shown; **B** zoom of the study area, the detailed geological background is modified from GTK Consortium (2006). * The profile of the conceptual circulation model is shown in Fig. 10; **C** simplified stratigraphy of the investigated area

iron–titanium oxides are also found. Rock fabrics are generally massive un-metamor-phosed with medium to very coarse or even pegmatitic grain sizes (Fig. 2C).

The overall hydrogeology of Mozambique was investigated by Ferro and Bouman (1987). Three main hydrogeological units, corresponding to geological units, were iden-tified: (1) aquifers related to the basement complex; (2) aquifers occurring in the Karoo formations and (3) aquifers related to the post-Karoo formations (Table 2). The base-ment complex covers about 60% of the country, occupying the western part of the cen-tral region and almost the entire region north of the Zambezi. The permeability of this complex is generally low. The permeability primarily depends on thickness and texture of the unit and presence of fractures and faults. The permeability of the Tete Suite is higher due to the intensive faulting and fracturing, whose effects are more pronounced on rocks formed by brittle and coarse-textured minerals (e.g., anorthosite). Moreover, good permeability may be found along dikes, where aquifers can develop in the fracture zone on the contact between the intrusive body and the adjacent rocks formations (Ferro and Bouman 1987). The hydrogeological properties of the Karoo formations are known only from a few limited areas. In general, the sequence is characterized by low permeability, although permeability is higher in fractured zones, coarse sandstones, fault-breccias and along intrusions. The post-Karoo formations have extremely variable permeability, from low to high. Higher values correspond to limestone and alluvial deposits, especially in the Zambezi delta (Ferro and Bouman 1987).

From a geochemical point of view, thermal springs in Mozambique, with water tem-perature between 40 and 95 °C, are known since the late seventies (Mc Nitt, 1978). These are located in the Niassa Province, where the temperatures reach the highest values (Metangula, 95 °C), Zambezia Province (Mossurie, Gilè, Maganja da Costa, Namacurra, Milange and Morrumbala Districts), where the temperatures of the water range from 45 to 75 °C. In the Tete Province water temperatures close to 80 °C were recorded, while the southern Sofala e Maniça Provinces show the highest number of thermal springs pre-senting, however, lower temperatures ranging from 27 to 58 °C (Martinelli et al. 1995).

In 2013 an extensive geochemical survey for geothermal exploration was car-ried out and the results have been briefly discussed on the Renewable Energy Atlas of

Table 2 Summary of Mozambique aquifers (modified from Groundwater Consultants Bee Pee (Pty) Ltd and SRK Consulting (Pty) Ltd 2002)

Aquifer system	Occurrence	Lithology	Permeability
Post-Karoo Formation	Most of southern part of the Country	Sandstones, limestones, conglomerates and alluvial deposits	Low productivity in sand-stone formations. High salinity waters (TDS up to 8500 mg/l). High yields in limestones (50–120 m^3/h) and alluvial plains (up to 200 m^3/h)
Karoo Formation	Limpopo, Rovuma and Zambezi valley	Clastic sedimentary units, basalts and rhyolites	Low yields (average 1.5 m^3/h) and very saline waters (TDS up 7000 mg/l)
Basement Complex	North and Centre of the Country	Metamorphosed and intrusive rocks	1–2 m^3/h occasionally up to 6 m^3/h. Fractures and faults may increase yields to 40–70 m^3/h

Mozambique (Gesto Energia 2014). In particular, 22 samples of water were collected from hot springs, mineral springs, water wells, rivers and sea, in six provinces: Manica, Tete, Nampula, Niassa, Zambézia and Sofala. Geothermometric evaluations indicated potential reservoir temperatures usable for electricity production in four sites: Boroma (164 °C), Morrumbala (153 °C), Maganja da Costa and Namacurra (155 °C). Moreover, the analysis of geophysical data allowed to identify areas with low resistivities that may indicate potential geothermal reservoirs at depths ranging between 1500 and 2500 m.

Liquid geothermometer evaluations based on the silica concentrations in thermal waters, reported by Martinelli et al. (1995) and the assumption of equilibrium with chalcedony, highlighted geothermal reservoir temperatures around 100–110 °C, somewhat lower than the aquifer temperatures proposed by Gesto (2014).

Methods

Sampling and laboratory analyses

Three thermal springs were sampled at *Nhawóndòc*, *Tenta* and *Mauira* (see Appendix A for photos) close to the *Missao de Boroma (Tete Province)*. These springs are located in remote areas, so that it was possible to sample them only with the help of local tribes. Water temperature, pH, Eh, electrical conductivity and alkalinity (titration with 0.05 N HCl) were determined in the field. Two aliquots of water were filtered (0.45 µm) and filtered + acidified (with HCl) for major anions (F^-, Cl^-, Br^-, SO_4^{2-} and NO_3^-) and cations (Ca, Mg, Na and K), respectively, and analyzed by ion-chromatography (Thermo Scientific ICS900). The analytical error was < 5%. A third aliquot was filtered and acidified (with HNO_3) for minor and trace elements (Sr, Fe, Mn, Al, B, Li) and analyzed by ICP-MS (Agilent 7500ce). Silica (SiO_2) was determined by molecular spectrophotometry on a filtered–diluted (1:10) sample. The analytical error for minor and trace elements was < 10%. In all sampled sites, sulfide was not smelled in the field, consistent with the absence of sulfide reducing filamentous bacteria storing white-colored elemental sulfur. Therefore, spring waters were not analyzed for the sulfide content.

The $\delta^{18}O$ and δD ratios (as ‰ vs. VSMOW) were determined by mass spectrometry (Analytical Precision AP 2003 and Finnigan MAT Delta plus, respectively). The analytical uncertainties were ± 0.1‰ for $\delta^{18}O$ and ± 1‰ for δD.

Samples for dissolved gas analyses were collected in glass flasks, and sealed by gas tight rubber/teflon plugs. Gases were extracted according to the method described by Capasso and Inguaggiato (1998) and analysed by gas chromatography (Varian micro GC 4900P). The analytical error was < 5%. Dissolved gas composition was calculated from the composition of the exsolved gas phase based on the Henry's law (Whitfield 1978).

The $\delta^{13}C$ ratio of total dissolved inorganic carbon (TDIC) (expressed as ‰ vs. VPDB) was analyzed by mass spectrometry (Finnigan Delta Plus) following the procedure described by Favara et al. (2002). The analytical uncertainly was ± 0.2‰.

The $\delta^{13}C$ and δD of CH_4 values (expressed as ‰ units vs. VPDB and VSMOW, respectively) were analyzed by mass spectrometry (Varian MAT 250) according to the method described by Schoell (1980). The analytical uncertainly was ± 0.15‰. The $^3He/^4He$ ratios (expressed as R/R_a, where R is the $^3He/^4He$ measured ratio and R_a is the $^3He/^4He$ ratio in the air: 1.39×10^{-6}; Mamyrin and Tolstikhin 1984), as well as the $^4He/^{20}Ne$ and $^{40}Ar/^{36}Ar$

ratios, were determined by mass spectrometer (VG 5400-TFT) according to the procedure described by Inguaggiato and Rizzo (2004). The analytical error was ± 1%.

Interpretation methods of geochemical data

Speciation–saturation calculations were performed using the PHREEQC code (Parkhurst and Appelo, 2013) and a modified version of the LLNL database as a preliminary step preceding the interpretation of geochemical data. This operation was necessary to separate the distinct components of total alkalinity and, in particular, the carbonate alkalinity, which is the sum of the concentrations (in equivalent units) of HCO_3^- and CO_3^{2-}, including related aqueous complexes, e.g., $CaHCO_3^+$, $MgHCO_3^+$, $CaCO_3^°$, and $MgCO_3^°$.

Following Cioni and Marini (2020), the chemistry of the thermal springs was investigated by means of triangular plots of major cations (i.e., Na, K, and Ca) and anions (i.e., Cl, SO_4, and carbonate alkalinity). Since these two triangular plots do not provide any information on total ionic salinity (Σ_{eq}), this parameter was examined using the binary diagram of Cl vs. $SO_4 + Alk_C$. In fact, the Σ_{eq} can be appreciated in the diagram, by comparing the position of each thermal water with the lines of slope -1 which are iso-Σ_{eq} lines (see Tonani et al. 1998 for further details). All these diagrams were prepared using concentrations in equivalent units, in contrast with the consolidated use of concentrations in weight units. The reason for this choice is that equivalent units are proportional to the amount of electrical charges carried by each ion and, therefore, are more suitable than weight units for the chemical classification of natural waters as recognized long ago (e.g., Zaporozec 1972 and references therein). Average seawater composition (Nordstrom et al. 1979) is also represented in the relevant plots for comparison.

Chloride diagrams and binary diagrams were inspected to assess the possible effects of different processes, such as mixing, precipitation of solid phases, and ionic exchange, on the solutes of interest.

Water geothermometry was performed using: (i) suitably selected, simple traditional solute geothermometric functions, (ii) multicomponent geothermometry, and (iii) the theoretical geothermometers of Cioni and Marini (2020).

In general, solute geothermometers have been used to estimate the temperatures of deep geothermal reservoirs starting from analyses of fluid samples collected at the surface from springs and exploration wells (Fournier 1977, 1989; Truesdell and Fournier 1977; Arnórsson and Gunnlaugsson 1985). These geothermometers link the equilibrium temperature of reference reactions to either the concentration of some dissolved components (e.g., SiO_2) or some concentration ratios (e.g., Na/K). Silica geothermometers are based on the temperature-dependent solubility of different silica minerals (i.e., quartz and chalcedony) which are presumably present as authigenic (secondary) solid phases in reservoir rocks and, therefore, in equilibrium with the aqueous solution. The quartz geothermometer is best for reservoir temperatures higher than 180 °C, whereas at lower temperatures, chalcedony rather than quartz probably controls the dissolved silica content (Arnórsson et al. 1983; Fournier 1989).

Multicomponent geothermometry was first proposed by Michard (1977), Michard and Roekens (1983), and Reed and Spycher (1984). Multicomponent chemical geothermometry comprises, as first step, the calculation of the saturation indices (SI's)

Procesi *et al. Geothermal Energy*   (2022) 10:2

Page 9 of 27

with respect to relevant hydrothermal minerals at the temperature of pH and alkalinity measurement. Then, temperature is increased in a series of steps and the SI's are recomputed at each step. Finally, the computed SI's are plotted against temperature. Since the geothermal liquid is presumably in equilibrium with the considered hydrothermal minerals at the aquifer temperature, ideally all the SI-temperature curves are expected to converge to zero at the aquifer temperature. Again, calculations were performed with the computer program PHREEQC (Parkhurst and Appelo, 2013) operating with the Lawrence Livermore National Laboratory (LLNL) database.

The theoretical Na–K, K–Ca and Na–Ca geoindicators of Cioni and Marini (2020) are based on the temperature dependence of the thermodynamic equilibrium constant of the exchange reactions involving pertinent hydrothermal minerals and take into account the average activities of relevant endmembers in solid solutions as well as Al–Si order–disorder on the tetrahedral sites of adularia.

The isotope data of H and O were interpreted to establish the origin of water and the possible effects of different processes (such as mixing and evaporation), whereas the infiltration elevation of rainwaters possibly involved in the recharge of the thermal circuits of interest cannot be evaluated due to the lack of isotope–elevation relationships specifically calibrated for the Tete area.

The C isotope data of CO_2 and CH_4 and the H isotope data of CH_4 were interpreted to assess the origin of these two C-bearing gases. To this purpose, the $\delta^{13}C$ value of gaseous CO_2 was computed from the measured $\delta^{13}C_{TDIC}$ values by means of the empirical equation of Zhang et al. (1995):

Equation (1) takes into account the equilibrium molar ratios of aqueous carbon species at sampling temperature and pH, computed with the PHREEQC code (Parkhurst and Appelo 2013), and the isotope equilibrium fractionation factors (ε) between dissolved carbonate species and gaseous CO_2 (Deuser and Degens 1967; Mook et al. 1974).

$$\delta^{13}C_{CO_2(g)} = \delta^{13}C_{TDIC} - \frac{H_2CO_3}{TDIC}\varepsilon_{(H_2CO_3-CO_2)} - \frac{HCO_3^-}{TDIC}\varepsilon_{(HCO_3^--CO_2)} - \frac{CO_3^{2-}}{TDIC}\varepsilon_{(CO_3^{2-}-CO_2)}$$
(1)

Then, the conceptual model of the geothermal system was elaborated inserting the results of the interpretation of geochemical data into the geological–hydrogeological framework of Tete area.

Results of chemical and isotopic analysis

Results of the chemical and isotopic analyses of sampled waters are listed in Table 3. Available data from literature (Martinelli et al. 1995) relative to one thermal spring (*Niaondive*) in the Tete Region were also discussed for comparison. Since pH is not reported by Martinelli et al. (1995), it was computed by the relation of Chiodini et al. (1991) for the P_{CO_2} given by the K–Ca–P_{CO_2} indicator (Giggenbach 1984) $5 \cdot 10^{-3}$ bar, and the chalcedony-temperature, 108 °C, obtaining the value of 7.8. The springs of *Nhawóndòc*, *Tenta* and *Niaondive* (indicated by codes 1, 2, and 4, respectively) have TDS values of approximately 1500 mg/L, slightly alkaline pH (7.8–8.0) and temperatures from 52 to 80 °C. The *Mauira* spring (code 3) shows slightly lower temperature

Procesi *et al. Geothermal Energy*   (2022) 10:2

Page 10 of 27

Table 3 Chemical and isotopic compositions of considered thermal waters and dissolved gases

Sample	Site	X	Y	Type	Elevation	T	TDS	pH	Eh	$\delta^{18}O$	δD	delta$^{13}C_{(TDIC)}$	F^-	Cl^-	Br^-	NO_3^-	PO_4^{3-}	SO_4^{2-}	HCO_3^-	Na^+	K^+	Mg^{2+}	Ca^{2+}	Li	B	Sr	SiO_2	Fe	Mn	Al	Ref
*	Luenha-Zambezi	33.79221	16.39026	mw	108	-	-	-	-	+0.21	+12.3	-	-	-	-	-	-	-	-	-	-	-	-	-	-	-	-	-	-	-	-	nd
1	Nhawóndóc	33.46192	16.00174	ts	158	66	1512	7.9	−209	-6.79	-44.8	-11.6	5.3	435	0.99	2.9	<0.10	372	128	363	29	1.5	98	0.34	0.29	2.3	98	14	19	131	nd
2	Tenta	33.44448	16.02411	ts	121	51	1460	8.0	−323	-6.75	-44.9	-13.0	6.1	442	0.63	0.87	<0.10	376	85	368	10	0.27	77	0.35	0.29	2.2	112	25	3.0	54	nd
3	Mauira1	34.15315	15.84933	ts	339	42	951	7.8	−404	-6.78	-42.7	-9.53	22	266	0.89	0.25	<0.10	66	231	268	21	0.10	8.2	0.32	0.76	0.09	75	609	47	584	nd
4	Niaondive	-	-	ts	-	80	1554	7.8	-	-	-	-	-	436	-	-	-	444	46	414	19	0.97	73	-	-	96	-	-	-	-	[1]

Sample	He	H_2	O_2	N_2	CO_2	CH_4	Ar	$R/Ra_{(C)}$	$\delta^{13}C(CO_2)$	$\delta^{13}C(CH_4)$	$\delta D(CH_4)$
1	0.00097	1.7E—05	0.23	1.1	0.030	0.00067	0.012	0.13	− 15.5		
2	0.00008	1.9E—06	0.22	0.82	0.024	0.00024	0.008	0.14	− 18.2	− 59	
3	0.00130	1.1E—05	0.14	0.75	0.029	0.00470	0.011	0.21	− 15.5		− 163

Coordinates (X, Y) WGS84 CGS; mw = meteoric water; ts = thermal spring; Elevation in meters; T in °C; Eh in mV; $\delta^{18}O$ and δD as ‰ vs. VSMOW; TDS, F^-, Cl^-, Br^-, NO_3^-, SO_4^{2-}, HCO_3^-, Na^+, K^+, Mg^{2+}, Ca^{2+}, Li, B, Sr and SiO_2 in mg/L; Fe, Mn and Al in µg/L; Ref: nd = new data, [1] = Martinelli et al., 1995; He, H_2, O_2, N_2, CH_4, CO_2 and Ar mmol/L; $\delta^{13}C$ in CO_2 and CH_4 as ‰ vs. VPDB; δD in CH_4 as ‰ vs. VSMOW
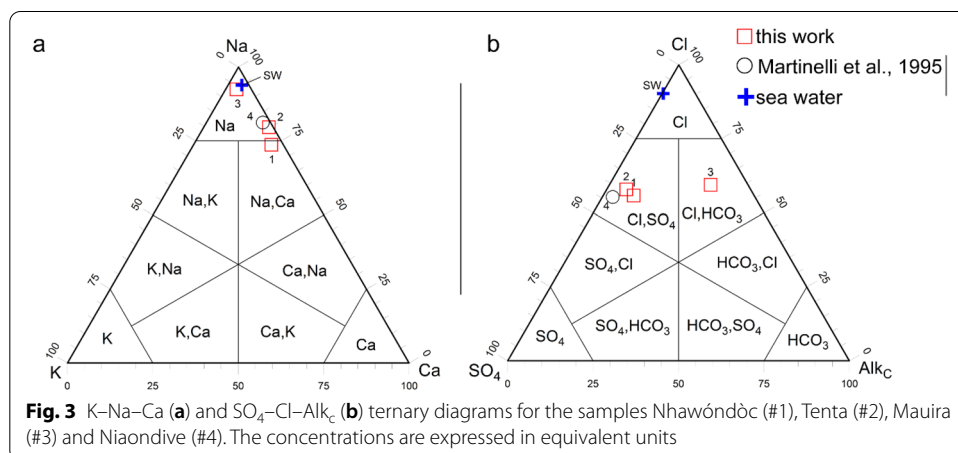
(42 °C) and TDS (952 mg/L) and similar pH (7.8). The redox potential is strongly negative for all the sampled waters, varying from -209 to -404 mV.
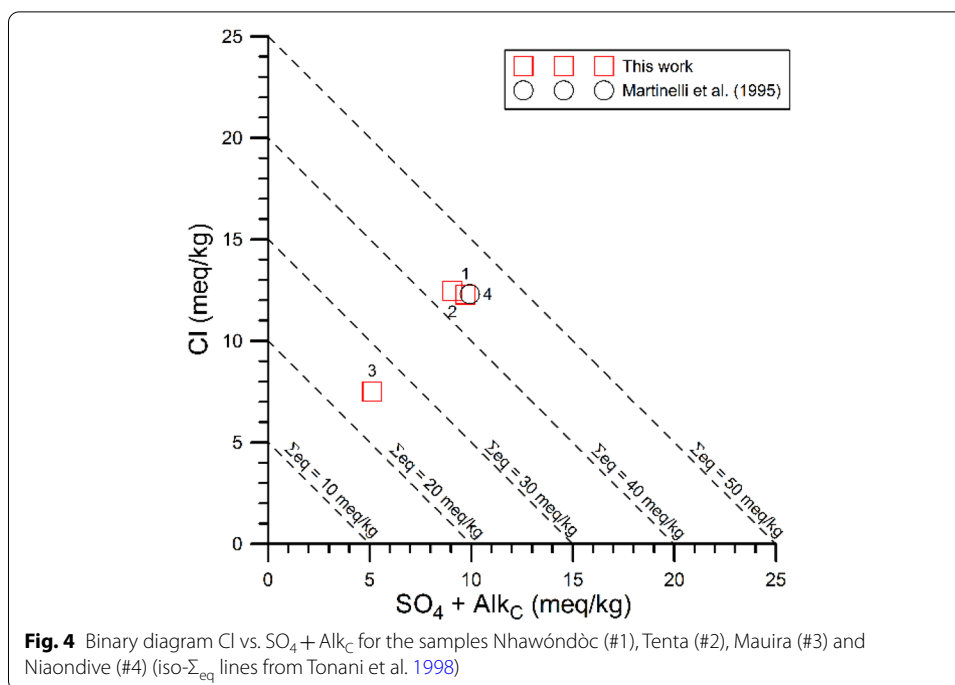
Speciation–saturation calculations at outlet temperatures indicate that carbonate alkalinity explains 89 to 99% of total alkalinity, while HCO_3^- and its aqueous complexes explain 93 to 99% of carbonate alkalinity. Therefore, the terms bicarbonate ion and carbonate alkalinity can be used in place of each other. Among the three main cations (Fig. 3a), Na^+ is the dominant one in all four samples, with relative concentrations of 73.7 to 92.4 eq%. The second major cation is Ca^{2+} in samples 1, 2, and 4, with relative concentrations of 16.6 to 22.8 eq%, but in sample 3 the relative concentration of K^+, 4.3 eq%, is weakly higher than the relative concentration of Ca^{2+}, 3.2 eq%. The comparison of relative chloride, sulphate and bicarbonate concentrations highlights the prevalence of Cl^- and SO_4^{2-} in samples 1, 2, and 4 and that of Cl- and HCO3- in sample 3 (Fig. 3b).

All in all, the three samples 1, 2, and 4 are similar to each other and are clearly separated from sample 3 in both triangular plots, indicating different chemical compositions, $Na–Cl(SO_4)$ and $Na–Cl(HCO_3)$, respectively. The binary diagram of Cl vs. $SO_4 + Alk_C$ (Fig. 4) shows that the three $Na–Cl(SO_4)$ samples are similar to each other also in terms of Σ_{eq} (42–45 meq/kg), whereas the $Na–Cl(HCO_3)$ sample 3 has significantly lower Σ_{eq} (25 meq/kg). Correlation diagrams highlights a good correlation between K and Cl, HCO_3 and Ca, and SO_4 and Na for the $Na–Cl(SO_4)$ samples.

The two different water types have distinct concentrations of some minor and trace constituents. In fact, the two $Na–Cl(SO_4)$ samples 1 and 2 have lower F, 5.3–6.1 mg/L, B, 0.29 mg/L, Fe, 14–25 µg/L and Mn, 3.0–19 µg/L, and higher SiO_2, 98–113 mg/L, Sr, 0.23–0.22 mg/L, whereas the $Na–Cl(HCO_3)$ sample 3 has higher F, 22 mg/L, and Fe, 609 µg/L, and lower SiO_2, 75 mg/L, and Sr, 0.09 mg/L.

Saturation indexes calculated at outlet temperatures indicate that all the thermal springs are undersaturated with respect to both anhydrite (SI from -2.78 to -0.78) and amorphous silica (SI from -0.54 to -0.29), whereas samples 1 and 2 are supersaturated with calcite (with SI of $+0.85$ and $+0.52$, respectively), sample 4 is close to saturation (with SI of $+0.02$), and sample 3 is slightly undersaturated (with SI of -0.21).
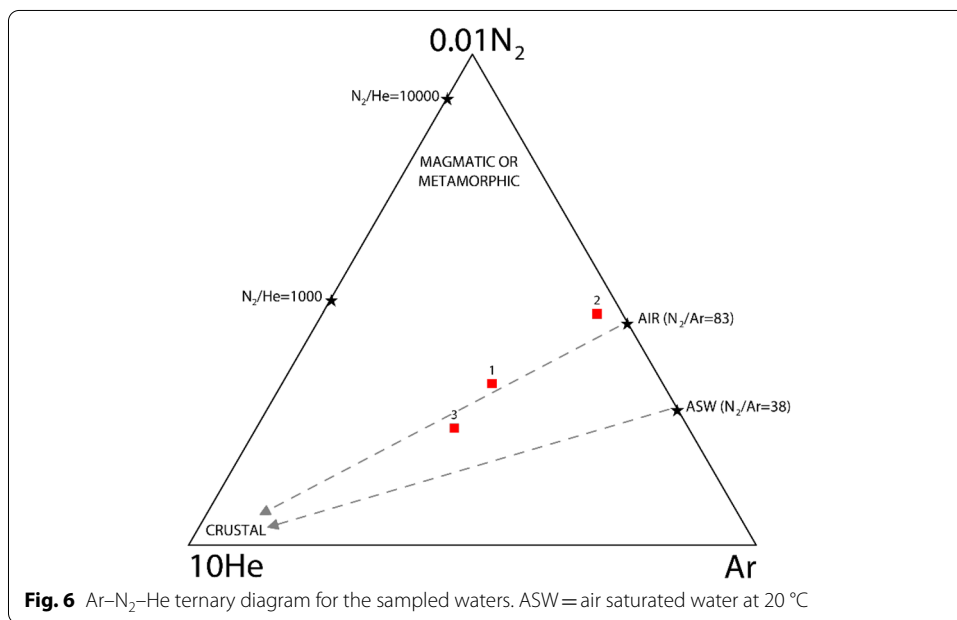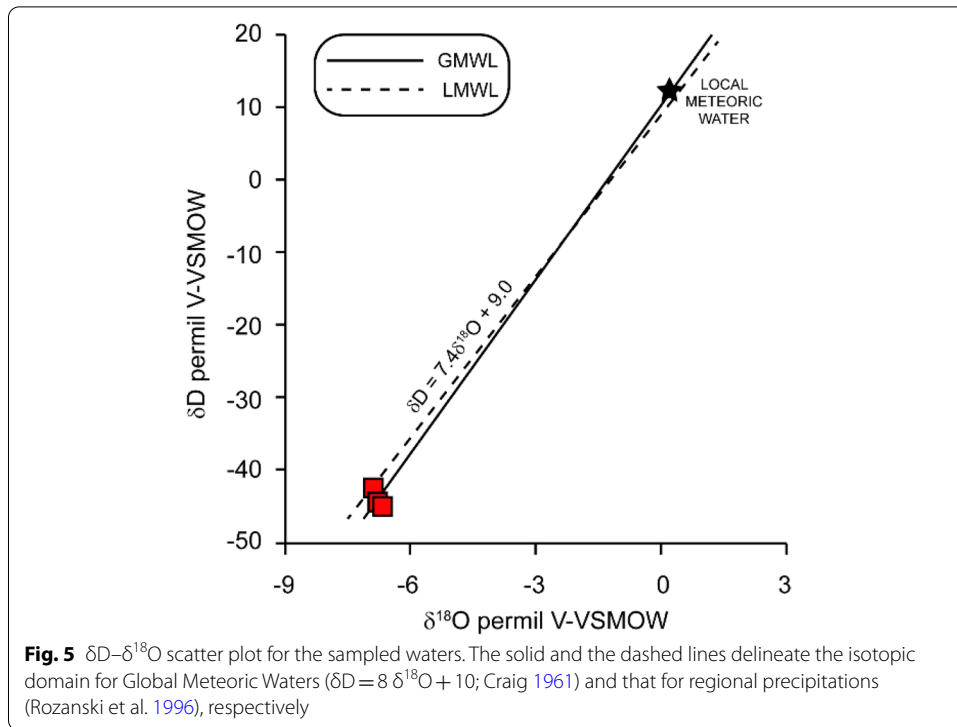

Fig. 3 K–Na–Ca (**a**) and SO_4–Cl–Alk_C (**b**) ternary diagrams for the samples Nhawóndòc (#1), Tenta (#2), Mauira (#3) and Niaondive (#4). The concentrations are expressed in equivalent units

Fig. 4 Binary diagram Cl vs. $SO_4 + Alk_C$ for the samples Nhawóndòc (#1), Tenta (#2), Mauira (#3) and Niaondive (#4) (iso-Σ_{eq} lines from Tonani et al. 1998)

The $\delta^{18}O$ and δD values of samples 1, 2, and 3 (Tab. 3) range from -6.79 to -6.75 and from -44.8 to $-42.7‰$ vs. VSMOW, respectively. The sample of rainwater, collected at Luenha in the Tete Region, has $\delta^{18}O$ and δD values of $+0.21$ and $+12‰$ vs. VSMOW, respectively. In the $\delta^{18}O$–δD diagram of Fig. 5, sampled waters plot between the Global Meteoric Water Line (Craig 1961) and the Regional Meteoric Water Line (Rozanski et al. 1996).

The composition of dissolved gases shows that N_2 is the main species (0.75 to 1.1 mmol/L) followed by O_2 (0.14 to 0.23 mmol/L), although the presence of these two gas constituents contrasts with the highly negative Eh values and is evidently due to air addition (Fig. 6). Carbon dioxide concentrations are constantly low (0.024 to 0.03 mmol/L) and somewhat higher than Ar concentrations (0.008 to 0.012 mmol/L), whereas a wide range of variation occur for CH_4 (0.24 to 4.7 µmol/L), He (0.08 to 1.3 µmol/L) and H_2 (0.002 to 0.017 µmol/L). Carbon monoxide is always below the instrumental detection limit. The $\delta^{13}C$–CO_2 values, calculated from Eq. (2), vary from -18.2 to $-15.5‰$ vs. VPDB (Table 3). The helium isotopic ratios, corrected for air contamination using the He/Ne ratio, range from 0.13 to 0.21 (Table 3).

Results of selected geothermometers
The results of selected traditional geothermometers and theoretical geothermometers of Cioni and Marini (2020) for the four thermal waters of interest are shown in Table 4, together with the outlet temperature and the degree of order–disorder of hydrothermal adularia, Z_{Adl}, in hypothetical equilibrium with the thermal waters of interest at the chalcedony temperature.

For the multicomponent geothermometry (Cioni and Marini, 2020), the saturation temperatures are given in Table 5. The considered hydrothermal minerals are quartz,

Fig. 5 δD–δ^{18}O scatter plot for the sampled waters. The solid and the dashed lines delineate the isotopic domain for Global Meteoric Waters (δD = 8 δ^{18}O + 10; Craig 1961) and that for regional precipitations (Rozanski et al. 1996), respectively

Fig. 6 Ar–N$_2$–He ternary diagram for the sampled waters. ASW = air saturated water at 20 °C

chalcedony, low-albite, two adularias of different order–disorder degree, muscovite, the four typical Ca–Al silicates of the neutral-pH suite (i.e., laumontite, clinozoisite, prehnite, and wairakite), clinochlore-7A, as well as heulandite, calcite, and anhydrite. Fluorite and barite are not considered, because their SI are scarcely informative having a weak temperature dependence.
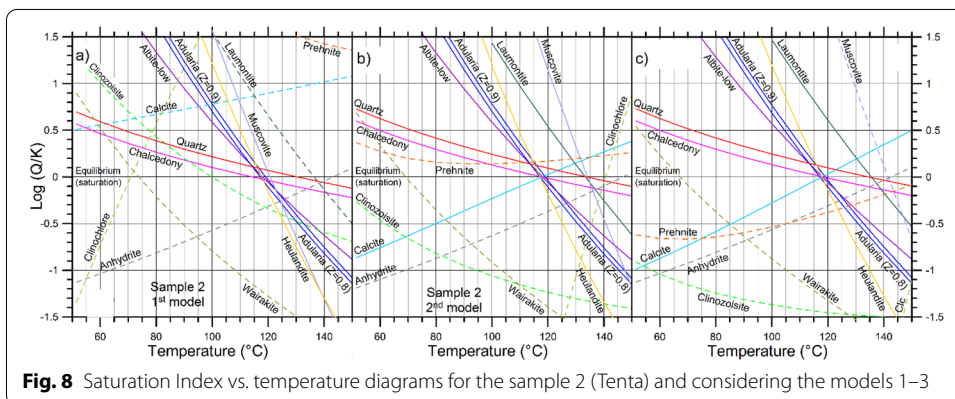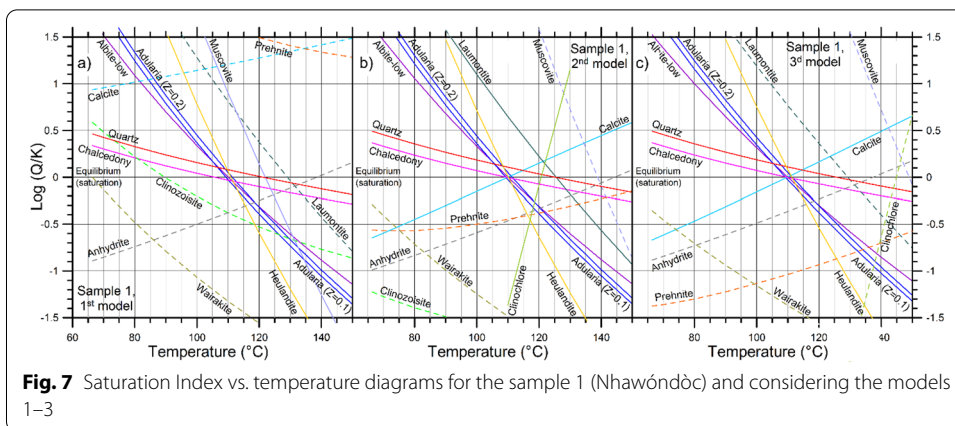
Table 4 Geothermometric results (°C) for the analysed thermal waters of the Tete area

Sample	Site	Outlet T	T_chc	T_qz	T_K–Mg
1	Nhawóndòc	66	110	136	119
2	Tenta	52	118	144	112
3	Mauira	42	93	121	153
4	Niaondive	80	108	135	113

Sample	Site	T Na–K (Z = 1)	T Na–K (Z = 0)	Z_{Adl}
1	Nhawóndòc	210	92	0.132
2	Tenta	132	27	0.848
3	Mauira	210	93	0.012
4	Niaondive	167	55	0.422

Sample	Site	T K–Ca,Czo	T K–Ca,Prh	T K–Ca,Lmt	T K–Ca,Wrk
1	Nhawóndòc	115	62	72	153
2	Tenta	127	91	90	154
3	Mauira	138	82	99	173
4	Niaondive	124	79	85	156

Sample	Site	T Na–Ca,Czo	T Na–Ca,Prh	T Na–Ca,Lmt	T Na–Ca,Wrk
1	Nhawóndòc	116	4	18	171
2	Tenta	134	46	30	177
3	Mauira	174	64	105	208
4	Niaondive	137	36	41	183

Table 5 Saturation temperatures indicated by multicomponent geothermometry for the three different models applied to samples 1 from Nhawóndòc, sample 2 from Tenta, and sample 3 from Maiura. Values within brackets are considered poorly reliable

Sample	Model	Albite-low and adularia	Calcite	Chalcedony	Clinochlore	Heulandite	Laumontite	Muscovite	Quartz
1	1	110	–	105.7	–	110.9	(129.1)	121.9	121.3
1	2	110	110	109.4	120.7	110.1	125.4	(138.9)	125.1
1	3	110	110	109.8	(144.9)	111.3	(129.3)	(149.0)	125.6
2	1	118	–	114.2	–	117.6	-	120.7	130.4
2	2	118	118	117.7	–	117.1	133.3	134.1	133.8
2	3	118	118	118.3	–	117.8	135.5	–	134.5
3	1	93	–	88.5	–	85.6	92.2	–	102.6
3	2	93	93	89.1	–	84.5	88.8	–	103.2
3	3	93	93	89.9	–	85.7	92.0	–	104.1

Clinochlore-7A, muscovite, clinozoisite, prehnite, and wairakite were assumed to have average activity based on the related solid solutions from drilled geothermal systems (Cioni and Marini 2020), whereas the other solid phases were assumed to be pure. Aluminum concentration was fixed by saturation with low-albite at the temperature indicated by the chalcedony geothermometer using the EQUILIBRIUM PHASES keyword data block of PHREEQC. Three different models were elaborated for the samples 1 from *Nhawóndòc*, 2 from *Tenta*, and 3 from *Maiura*. In the first model, the sample was simply heated from the outlet temperature to the maximum temperature of 150 °C, at fixed

Fig. 7 Saturation Index vs. temperature diagrams for the sample 1 (Nhawóndòc) and considering the models 1–3

Fig. 8 Saturation Index vs. temperature diagrams for the sample 2 (Tenta) and considering the models 1–3

steps of 10 °C, apart from the first one whose magnitude depends on the outlet temperature. The REACTION TEMPERATURE keyword data block of PHREEQC was utilized to this purpose. Since the aqueous solutions resulted supersaturated with calcite, saturation with calcite at the temperature given by the chalcedony geothermometer was imposed in the second and third models following two distinct approaches. In the second model, calcite equilibrium was attained by precipitation of a suitable amount of calcite, using the EQUILIBRIUM PHASES keyword data block of PHREEQC, whereas in the third model, calcite equilibrium was achieved by addition of an appropriate quantity of gaseous CO_2, at fixed partial pressure, using the GAS PHASE keyword data block of PHREEQC. The SI vs. temperature diagrams for three models elaborated for the samples 1 from *Nhawóndòc*, 2 from *Tenta*, and 3 from *Maiura*, are shown in Figs. 7, 8, and 9, respectively.

Discussion

Processes governing the chemical and isotopic composition of waters

Water–rock interaction at relatively high temperature may be considered as the main process influencing the chemical composition of the collected waters. The Na–Cl(SO₄) composition of thermal springs at *Nhawóndòc*, *Tenta* and *Niaondive* suggests an interaction with low solubility rocks, i.e., gneisses and granitoid rocks of the Crystalline

Fig. 9 Saturation Index vs. temperature diagrams for the sample 3 (Mauira) and considering the models 1–3
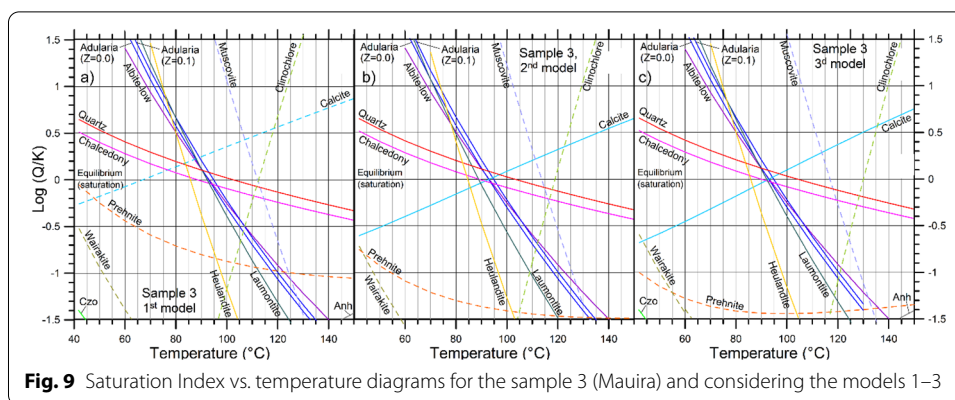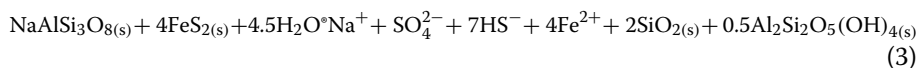
Basement and mafic rocks of the Tete Suite. In fact, the relatively low salinity of waters seems to exclude the interaction with soluble evaporitic rocks and/or mixing with highly saline (connate) waters, which are not reported to be present in the study area. So, the relatively high Cl^- concentration may result from the dissolution of minerals in which the Cl^- ion occurs as a vicariant of OH^-, such as micas (mainly biotite, as accessory mineral in the gneisses of the study area), amphiboles, apatite, etc. Consistently, the relatively high SO_4^{2-} concentrations may be produced through pyrite dissolution under O_2-free conditions. Owing to its deleterious environmental impact, the reaction mechanisms and kinetics of O_2-driven pyrite dissolution has received considerable attention (e.g., Moses et al. 1987; Moses and Herman 1991; Williamson and Rimstidt 1994; Gleisner et al. 2006), whereas pyrite dissolution in O_2-free systems has never been investigated to the best of our knowledge. Since the formal oxidation state of S in pyrite is -1, it is reasonable to hypothesize, from a purely theoretical point-of-view, the occurrence of the following disproportionation reaction in the absence of O_2:

$$4FeS_2 + 4\,H_2O°H_2S_{(aq)} + 6\,HS^- + SO_4^{2-} + 4\,Fe^{2+}. \tag{2}$$
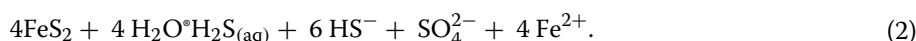
According to reaction (2), seven of the eight S atoms initially hosted in pyrite are reduced to aqueous sulphide species (in which the oxidation state of each S atom is − 2), with the gain of seven electrons and only one is oxidized to sulphate (in which the oxidation state of S is + 6), with the loss gain of seven electrons. In contrast, Fe is expected to maintain the formal oxidation state of + 2, under strongly reducing conditions. Sulphide and sulphate are considered in reaction (2), because they are the thermodynamically most stable sulfur species (Langmuir 1977), although several aqueous S species with formal oxidation state intermediate between those of sulphide and sulphate are known (Williamson and Rimstidt 1992) and could be involved in pyrite disproportionation in the absence of O_2.
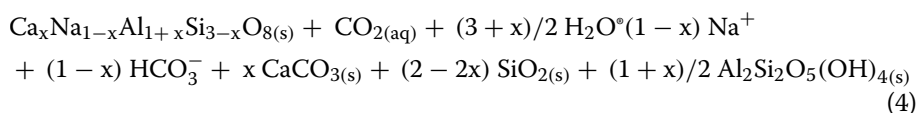
It must be underscored that reaction (2) produces aqueous H_2S, which is an acid somewhat weaker than aqueous CO_2 (or carbonic acid) below 115 °C. However, H_2S becomes an acid stronger than aqueous CO_2 at higher temperatures. Therefore, pyrite dissolution in O_2-free systems might actually generate the acidity needed for the occurrence of silicate dissolution, thus playing a fundamental role in the overall water–rock interaction process. The good correlation between SO_4 and Na for the three Na–Cl(SO_4) samples

could be explained by coupled pyrite–albite dissolution, as schematically indicated by the following disproportionation reaction:

$$NaAlSi_3O_{8(s)} + 4FeS_{2(s)} + 4.5H_2O°Na^+ + SO_4^{2-} + 7HS^- + 4Fe^{2+} + 2SiO_{2(s)} + 0.5Al_2Si_2O_5(OH)_{4(s)} \tag{3}$$

Reactions (2) and (3) must be considered working hypotheses at this stage. To confirm their occurrence, we suggest to investigate the distribution of pyrite in the rocks of the area of interest (no such data are available at present to the best of our knowledge) and to carry out sulphur isotopic analyses, as done for several thermal sites of Malawi (unpublished reports by LM). The good correlation between HCO_3^- and Ca^{2+} for the three Na–Cl(SO_4) samples suggests the occurrence of calcite dissolution/precipitation which, in turn, is probably controlled by acquisition/loss of CO_2. The good correlation between K^+ and Mg^{2+} is probably explained by acquisition of both constituents upon cooling or occurrence of exchange reactions also involving Na^+ ion. The possible occurrence of these processes casts some uncertainties on theoretical geothermometric evaluations.

The *Maiura* Na–Cl(HCO_3) spring (#3) is located in an area marked by the presence of rocks belonging to the Karoo and Post-Karoo Formations, largely made of sedimentary rocks with coal-bearing horizons. In this framework, the availability of CO_2 is expected to be higher than in the mafic rocks of the Tete Suite and the underlying crystalline rocks of the Precambrian basement. Therefore, CO_2-driven plagioclase dissolution, at saturation with calcite is expected to be the main reaction leading to the production of Na–Cl(HCO_3) waters (Eq. 4):

$$Ca_xNa_{1-x}Al_{1+x}Si_{3-x}O_{8(s)} + CO_{2(aq)} + (3+x)/2\,H_2O°(1-x)\,Na^+$$
$$+ (1-x)\,HCO_3^- + x\,CaCO_{3(s)} + (2-2x)\,SiO_{2(s)} + (1+x)/2\,Al_2Si_2O_5(OH)_{4(s)} \tag{4}$$

These waters are typically characterized by low Ca^{2+} concentrations, owing to saturation with calcite and high HCO_3^- concentrations. Consequently, they may acquire high F^- concentrations, up to the maximum value constrained by fluorite saturation, through dissolution of minerals in which the F^- ion occurs as vicariant of OH^- ion, such as apatite, micas, amphiboles, etc. Highly saline waters (over 8000 mg/L) were found in the Karoo and Post-Karoo Formations (Groundwater Consultants Bee Pee (Pty) Ltd and SRK Consulting (Pty) Ltd 2002) but the low salinity of the *Maiura* spring seems to exclude the hypothesis of mixing with similar brines.

Actually, the Cl concentration of *Maiura* spring, 266 mg/L, is significantly lower than those of samples 1, 2, and 4, 435–442 mg/L, probably indicating that the extent of water–rock interaction (and consequently the residence time of the water in the subterranean circuit) is lower at *Maiura* compared to the other three sites, even though the Cl source is dissolution of minerals with Cl^- ions substitute OH^- ions.

The following observations can be drawn for the minor and trace elements: (i) Both Li and B concentrations are low in all three samples 1, 2, and 3, which are consequently positioned close to the chloride vertex in the triangular plot of Cl–B–Li (not reported) and far from the rock dissolution area. This spread of samples suggest that only Cl has mobile behaviour, whereas B and Li have non-conservative behaviour due to either

incorporation into precipitating secondary minerals (e.g., clay minerals) or sorption onto solid phases as observed elsewhere for Li (Brozzo et al. 2011). (ii) Sample 3 has Cl/Br mass ratio of 299, which is similar to the average seawater value of 288, whereas samples 1 and 2 have higher Cl/Br mass ratios, 439 and 702, respectively, possibly due to Br sorption on Al–Fe oxyhydroxides (Chubar et al. 2005) or other ion exchangers. (iii) Sample 3 has Sr and Mg concentrations significantly lower than those of samples 1 and 2, probably due to incorporation of both alkaline earth metals in precipitating calcite (Paquette and Reeder 1995).

The $\delta^{18}O$ and δD values of the collected waters, indicating a meteoric origin, are consistent with the lack of saline (connate) waters from the deeper circuits. The slightly less negative δD value of sample 3, -42.7 ‰, compared to those of samples 1 and 2, -44.8 and -44.9 ‰, suggests that the average recharge elevation might be weakly lower at Mauira compared to the other two sites. The $\delta^{18}O$ and δD values of the three thermal waters are significantly lower than those of the local rainwater sample indicating that the rainwaters recharging the thermal circuits infiltrate at elevations considerably higher than the 108 m asl of the site, where the rainwater sample was collected, although a number of rainwater samples collected at different elevations are needed to constrain the isotope–elevation relationship.

As far as the dissolved gases are concerned, the classical triangular diagram of N_2–Ar–He (Fig. 6; from Giggenbach and Goguel 1989) shows that N_2 and Ar are mostly of atmospheric origin and are driven to depth by infiltrating meteoric waters. The relatively high He contents of samples 1 and 3 point to a prolonged residence time in crustal rocks, leading to accumulation of radiogenic ^4He produced from α-decay of U- and Th-bearing minerals. The crustal origin of He is confirmed by the low R/R_a ratios (0.13–0.21 R/R_a), based on which it is reasonable to conclude that there is no evidence of primary mantle ^3He degassing (Marty and Jambon 1987). Carbon dioxide shows very low concentrations in the collected waters. The isotopic composition suggests a shallow origin from plant–root respiration and aerobic decay of organic matter contained in soils and/or a deeper one through anaerobic decay of organic matter contained in the sedimentary rocks of the Karoo Supergroup (Cerling et al. 1991), whereas a deep (inorganic) magmatic–metamorphic provenance seems to be ruled out. Shallow alteration of organic matter and/or interaction with coal deposits of the Lower Karoo Formation may be responsible for the relatively high CH_4 content of the *Maiura* spring relative to the other samples. This hypothesis is consistent with the carbon and hydrogen isotopic composition of CH_4, which suggests a probable derivation of methane from biogenic sources.

Geothermometric estimations

Silica geothermometers are potentially affected by dilution, but the effects of this process are expected to be negligible for the Na–Cl(SO_4) thermal springs at *Nhawóndòc*, *Tenta* and *Niaondive* (samples 1, 2 and 4, respectively), because they have very similar chloride concentrations and are practically superimposed in the binary diagram of Cl vs. $SO_4 + Alk_C$ (Fig. 4), suggesting that these springs discharge the same pure thermal

endmember. This assumption is fortified by the low concentrations of Mg recognized in the samples and suggesting the negligible presence of shallow fluids. The limited differences in SiO_2 concentrations are probably due to variable re-equilibration upon cooling during their upflow. Chalcedony solubility (Fournier 1977) indicates aquifer temperatures of 110, 118, and 108 °C for samples 1, 2 and 4, respectively, and a somewhat lower aquifer temperature, 93 °C, for the *Maiura* spring, (sample 3) (Table 4). Corresponding quartz temperatures (Fournier 1977) are 26–28 °C higher than chalcedony temperatures and, therefore, are probably less likely than latter ones (see Sect. 4.2). The K–Mg geothermometer (Giggenbach 1988) provides aquifer temperatures of 119, 112, and 113 °C for samples 1, 2 and 4, respectively, in good agreement with chalcedony temperatures, whereas the K–Mg temperature of sample 3, 153 °C, is significantly higher than the chalcedony temperature, probably due to Mg incorporation in precipitating calcite (see above).

As shown by Cioni and Marini (2020), all the different Na–K geothermometric functions proposed by different authors appear to be plausible and, therefore, there is an infinite number of Na–K geothermometers which are controlled by the exchange reaction between low-albite and variably ordered adularia, from fully ordered maximum–microcline (with order–disorder degree, $Z_{Adl} = 1$) to completely disordered high-sanidine (with $Z_{Adl} = 0$). Equilibrium coexistence of low-albite and fully ordered maximum–microcline indicates aquifer temperatures of 210, 132, and 167 °C for samples 1, 2 and 4, respectively, whereas equilibrium coexistence of low-albite and completely disordered high-sanidine indicates aquifer temperatures of 92, 27, and 55 °C for samples 1, 2 and 4, respectively (Table 4). The limiting Na–K aquifer temperatures of sample 3 compare with those of sample 1, that is, 210 and 93 °C. Since there is an infinite number of Na–K geothermometers, there is also an infinite number of other cation geothermometers which are controlled by exchange reactions involving adularia. For this reason, cation geothermometers (e.g., K–Mg, Na–K–Ca, etc.) appear to be less reliable than silica geothermometers, in general.

Following Cioni and Marini (2020) and using the Na–K ratio as indicator of the degree of order–disorder of hydrothermal adularia, in hypothetical equilibrium with the thermal waters of interest at the chalcedony temperature, it turns out that Z_{Adl} is 0.132, 0.848, and 0.422, for samples 1, 2 and 4, respectively, and 0.422 for sample 3. These Z_{Adl} values can then be used to compute K–Ca and Na–Ca temperatures, controlled by clinozoisite (Czo), prehnite (Prh), laumontite (Lmt), and wairakite (Wrk). For the three Na–Cl(SO$_4$) thermal springs at *Nhawóndòc*, *Tenta* and *Niaondive*, the most plausible K–Ca and Na–Ca temperatures (i.e., closest to the chalcedony temperature) are those controlled by equilibrium with clinozoisite, namely, 115, 127, and 124 °C and 116, 134, and 137 °C, for samples 1, 2 and 4, respectively. For the Na–Cl(HCO$_3$) *Maiura* spring (sample 3), the most plausible K–Ca and Na–Ca temperatures are those controlled by equilibrium with laumontite, namely, 99 and 105 °C, respectively. All in all, these K–Ca and Na–Ca temperatures are somewhat higher

than chalcedony temperatures. Among the three Na–Cl(SO$_4$) thermal springs, sample 1 from *Nhawóndòc* is the one with the K–Ca and Na–Ca temperatures closest to the chalcedony temperature, with differences of 5 and 7 °C only. Since this is the sample with the highest Ca concentration, 98.1 mg/kg (vs. 77.1 and 73.7 mg/kg of samples 2 and 4, respectively), the deviations of the K–Ca and Na–Ca temperatures from the chalcedony temperature might be due to variable loss of Ca, probably through precipitation of calcite, as suggested by Ca–HCO$_3$ relationships (see above).

Regarding multicomponent geothermometry, the obtained SI–T curves (Figs. 7, 8, 9) are very different from each other, for clinozoisite, prehnite, muscovite, and clinochlore-7A, whereas the SI–T curves of quartz, chalcedony, the two adularias, low-albite, laumontite, wairakite, heulandite, and anhydrite exhibit smaller shifts.

In all three samples, clinozoisite, prehnite, wairakite, and anhydrite do not attain the equilibrium condition within the saturation range of SiO$_2$ minerals. The deviation from this condition for the Ca–Al silicates could be due to variable loss of Ca and/or the fact that the SI of Ca–Al silicates is strongly influenced by the pH and partial pressure of CO$_2$, which are poorly defined parameters, at high temperatures, for the thermal springs. The occurrence of hydrothermal anhydrite requires SO$_4$ concentrations higher than those of the thermal waters of interest. These minerals are, therefore, poor geothermometric indicators, at least in the considered waters.

Clinochlore-7A and muscovite achieve saturation at different temperatures, either close to the quartz equilibrium temperature in some cases or at even higher temperatures in other cases. The geothermometric indications provided by these two minerals have to be considered with caution due to the variable chemistry of hydrothermal chlorites and illites.

Laumontite attains saturation close to the quartz equilibrium temperature in samples 1 and 2 and near the chalcedony saturation temperature in sample 3. Heulandite achieves saturation near the chalcedony equilibrium temperature in samples 1 and 2 and at somewhat lower temperatures in sample 3.

Low-albite, the two adularias, and heulandite (as well as, obviously, calcite in the second and third models) attain the equilibrium condition within the saturation temperatures of quartz and chalcedony. Since equilibrium with low-albite and calcite (in the second and third models) was forced and the order parameter of the two adularias was suitably chosen, the only independent geothermometric results are given by chalcedony, quartz, and heulandite. Since quartz probably overestimate the aquifer temperature below 180 °C (Arnórsson et al. 1983), the results given by multicomponent geothermometry are essentially based on chalcedony and heulandite saturation, with mean values of 109.5 $\pm$ 2.0 (1σ) °C for sample 1, 117.1 $\pm$ 1.5 °C for sample 2, and 87.2 $\pm$ 2.2 °C for sample 3. These temperatures are slightly lower than those given by the chalcedony geothermometer of Fournier (1977), 110, 118, and 93 °C, respectively, because pH effects (and the heulandite saturation temperature) are considered in multicomponent geothermometry, whereas they are neglected by the chalcedony geothermometer.

Fig. 10 Conceptual circulation model for the Tete area. The trace of the geological section and the relative geological map are shown in Fig. 2B
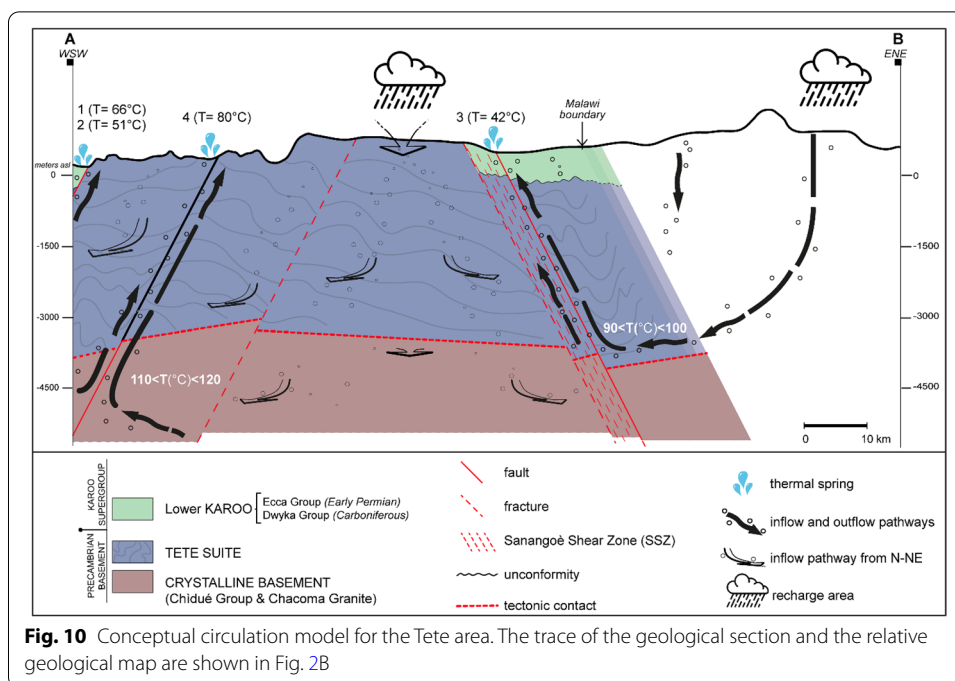
All in all, the temperature estimated by multicomponent geothermometry and based on chalcedony and heulandite saturation are fairly consistent with those provided by chalcedony solubility, the K–Mg geothermometer, and the K–Ca and Na–Ca theoretical geothermometers for samples 1, 2 and confirm that these two thermal waters discharge from a thermal aquifer at temperature of 110–120 °C, whereas sample 3 comes from an aquifer at 90–100 °C. Nevertheless, since these geothermometric estimations are entirely based on spring water samples, it is necessary to confirm these results by means of data acquired through deep drillings to be carried out in future.

Conceptual circulation model

By considering the chemical and isotopic composition of the waters, the geothermometric evaluations and the available geological and hydrogeological information, a conceptual circulation model is proposed for the study area (Fig. 10). Meteoric waters infiltrating through the widespread fracture network of the SSZ circulate for more than 2 km deep in the crust, namely, into the Precambrian Basement. The crustal origin of He (as indicated by the low R/R_a ratios) and the relatively high He contents in the dissolved gas phase provide further evidence for the long circulation underground. The heavier isotopic values of the rainwater sample relative to the thermal springs suggest that the recharge area may be located at higher altitudes than the sampling quote (~ 100 m asl). The recharge area may correspond to the hills and mountains (up to 1000 m asl) located N and/or E of the study area (Fig. 10) towards Malawi (Fig. 2A), but this inference is

poorly constrained due to the lack of an isotope–altitude relation for the study area. Meteoric waters flowing down into the crust are heated up to maximum temperatures of 110–120 °C below sites 1, 2, and 4, and 90–100 °C below site 3. There is a large uncertainty on the depths reached by the infiltrating meteoric waters owing to the poor knowledge of the local geothermal gradient. For instance, the median geothermal gradient of Mozambique is 19.2 °C/km, while the 25th and 75th percentiles are 18.1 and 21.2 °C/km, respectively (Jennings et al. 2022 and references therein). Adopting these values and an average annual temperature of 26.1 °C at the surface, the temperatures of 110–120 °C are expected to be present at depths of 4.4–4.9 km (possible range 4.0–5.2 km) below sites 1, 2, and 4, whereas the temperatures of 90–100 °C are estimated to be found at depths 3.3–3.8 km (possible range 3.0–4.1 km) below site 3. After a residence time at these depths long enough for the attainment of the thermo-chemical water–rock equilibrium, the heated fluids rise up quickly towards the surface, via fractures and faults. In fact, rock permeability is mostly related to fractures and faults, which drive at the same time the meteoric water downwards and deep waters upwards, according to the position of the fluids in the convective cells.

Water–rock interaction processes at high temperature between the fluids and the metamorphic and mafic rocks control the chemical composition of the deep waters that are finally discharged from the considered thermal springs. The described hydrothermal system does not show connections with any active magmatic system but it seems to be related to a paleo-suture tectonic structure, as observed in intra-cratonic systems (Minissale et al. 2000). This hypothesis agrees with: (1) the low CO_2 concentrations and the negative $\delta^{13}C$ value of CO_2, (2) the isotopic value of CH_4, (3) the relatively high He contents and the low R/R_a ratios, indicating low ^3He concentrations, and (4) the N_2/Ar ratio close to the meteoric value.

The conceptual model described above must be considered as a tentative conceptual model of fluid circulation. It is necessary to study additional thermal springs, especially in the area of the Maiura spring, and to acquire fluid samples from drilled boreholes, to confirm these first conclusions.

Conclusions

Mozambique is endowed with a variety of natural resources but it suffers for both improper use and extremely low access to energy in a sustainable manner. At present only 13% of the population has access to electricity. In this framework, the development of the geothermal energy, currently unexploited, may represent an important goal to contribute to economic growth of the country. Combining the results of the geochemical survey and the geological–structural and hydrogeological settings, the conceptual circulation model was defined for the Tete geothermal system. The study area, located in the northwestern part of Mozambique, is characterized by the presence of some thermal springs with temperature at the emergence up to 80 °C. The main identified geothermal reservoir is hosted in the Precambrian Basement constituted by the Tete Suite and the Crystalline Basement. The fluids have a meteoric origin, as indicated by $\delta^{18}O$ and δD values, and are characterized by relatively low salinity and no-aggressive gas components. Their chemical composition is related to water–rock interaction processes with metamorphic and mafic rocks. The large convective circulation is well developed along

Procesi *et al. Geothermal Energy*   (2022) 10:2

Page 23 of 27

Table 6 Features summary of the potential geothermal system located in the Tete area

Main Geothermal Reservoir	Geological Formation	Thickness (m)	Permeability	Estimated temperature (°C)	Type of geothermal system	Chemical features of the fluid	Potential use of the resource
Precambrian Basement	Tete Suite	1500 ÷ 2000	Secondary permeability related to fractured–faulted rocks and dikes	90 ÷ 100	Igneous, basement-type geothermal play sensu Moeck (2014) or unconventional Geothermal System (e.g, Enhanced Geothermal System—EGS)	- Na–Cl - low TDS - no corrosive gas phases	Direct Use: livestock farming, agriculture, pasteurization, beet sugar extraction, distilled liquor, lumber, ecc Indirect Use: power generation by binary cycle and/or conventional flash plants
	Crystalline basement	> 2000		110 ÷ 120			

fractures and faults, connected mainly to the Sanangoè Shear Zone. The maximum esti-mated temperature of the reservoir fluids ranges from 110 to 120 ℃ below sites 1, 2, and 4, whereas the temperature below site 3 is around 90–100 ℃. These temperatures are related to a deep aquifer hosted in the Crystalline Basement and the Tete Suite, respec-tively. The heating of the fluids is apparently connected to a relatively low geothermal gradient, 19.2 ℃/km only, implying that the meteoric waters recharging the geothermal circuit have to descend to comparatively high depths, in the order of 4.4–4.9 km below sites 1, 2, and 4, and 3.3–3.8 km below site 3. These findings are preliminary being largely based on the analysis of spring waters, while more robust results could be acquired by deep drilling. Nevertheless, according to these findings and the chemical and isotopic composition of fluids, we can exclude any connection with active magmatic systems.

The above described characteristics of the Tete geothermal system (i.e., discrete permea-bility and circulation along fractures-faults, relatively low geothermal gradient and absence of a heat source) allows one to consider it as an igneous, basement-type geothermal play sensu Moeck (2014) or as an unconventional geothermal system, similar to the Enhanced Geothermal Systems (EGS). The system may be exploited for several geothermal uses, both direct and indirect, such as agriculture, pasteurization, beet sugar extraction, distilled liq-uor and/or power generation by binary cycle or conventional flash plants (Table 6). In par-ticular, the geothermal reservoir hosted into the crystalline basement could be exploited for indirect uses, whereas the Tete Suite is more suitable for direct utilization. Moreover, the low salinity of the fluids and the absence of corrosive gas components could be a warranty for a long duration of eventual industrial plants established in such area. Nevertheless, a suitable selection of materials must be performed to avoid corrosive effects, such as the chloride stress corrosion cracking of austenitic stainless steel, owing to the comparatively high chloride concentrations. Moreover, the scaling potential must also be assessed, in view of the relatively high concentrations of SiO_2 and HCO_3.

We think that further zones could have similar features as the Zumbo area located west-ward from Tete city, close to the Zambia border. Additional studies should be carried out to better understand the geothermal systems of Mozambique and to allow strategic energy planning and an improvement of the energy network. The use of geothermal resources in Mozambique could greatly improve and fortify the energy distribution in the country, increasing local distribution especially in the areas in proximity to the potential geother-mal fields, such as the city of Tete and its hinterland. These represent expanding areas with many factories and companies that suffer from intermittent energy distribution and that could find in geothermics a precious energy source.

Appendix A
See Fig. 11.

Procesi *et al. Geothermal Energy* (2022) 10:2

Page 25 of 27

Fig. 11 Photos of the sampled thermal springs located close to Tete City

Availability of data and materials

Not applicable.

Procesi *et al. Geothermal Energy* (2022) 10:2

Page 26 of 27

Declarations

Competing interests
The authors declare that they have no competing interests.

Author details
[1]Istituto Nazionale Di Geofisica e Vulcanologia, Rome, Italy. [2]Steam Group, Pisa, Italy. [3]Energy Technologies and Renewable Sources Department, ENEA, Rome, Italy.

References

Aquater. Study for high and low enthalpy in Zambezia Province and adjacent areas of Tete, Sofala and Manica Provinces. Preliminary Geothermal Reconnaissance, S.Lorenzo in Campo; 1980. p. 16.

Arnórsson S, Gunnlaugsson E, Svavarsson H. The chemistry of geothermalwaters in Iceland. III. Chemical geothermometry in geothermal investigations. Geochim Cosmochim Acta. 1983;47:567.

Arnórsson S, Gunnlaugsson F. New gas geothermometers for geothermal exploration—calibration and application. Geochim Cosmochim Acta. 1985;49:1307–25.

BRGM. Project de exploration geothermique an Mozambique. Technical report, Orleans Cedex; 1980. p. 12.

Brozzo G, Accornero M, Marini L. The alluvial aquifer of the Lower Magra Basin (La Spezia, Italy): conceptual hydrogeochemical-hydrogeological model, behaviour of solutes, and groundwater dynamics. Carbonates Evaporites. 2011;26:235–54.

Capasso G, Inguaggiato S. A simple method for the determination of dissolved gases in natural waters. An application to thermal waters from Vulcano Island. Appl Geochem. 1998;13:631–42.

Cerling TE, Solomon DK, Quade J, Bowman JR. On the isotopic composition of carbon in soil carbon dioxide. Geochim Cosmochim Acta. 1991;55:3403–5.

Chambal H. Energy security in Mozambique. Series on trade and energy security—policy report 3. International Institute for Sustainable Development; 2010. p. 28.

Chiodini G, Cioni R, Guidi M, Marini L. Chemical geothermometry and geobarometry in hydrothermal aqueous solutions: a theoretical investigation based on a mineral-solution equilibrium model. Geochim Cosmochim Ac. 1991;55:2709–27.

Chubar NI, Samanidou VF, Kouts VS, Gallios GG, Kanibolotsky VA, Strelko VV, Zhuravlev IZ. Adsorption of fluoride, chloride, bromide, and bromate ions on a novel ion exchanger. J Colloid Interf Sci. 2005;291:67–74.

Cioni R, Marini L. A thermodynamic Approach to Water Geothermometry. Springer; 2020. https://doi.org/10.1007/978-3-030-54318-1.

Craig H. Isotopic variations in meteoric waters. Science. 1961;133:1702–3.

Deuser WG, Degens ET. Carbon isotope fractionation in the system CO_2 (gas)-CO_2 (aqueous)-HCO_3 (aqueous). Nature. 1967;215:1033–5.

Gesto Energia. Renewable energy atlas of Mozambique, ISBN 978-989-97416-3-8, (1st Edition). 2014.

Favara R, Grassa F, Ingaggiato S, Pecoraino G, Capasso G. A simple method to determine the $\delta^{13}C$ content of total dissolved inorganic carbon. Geofis Int. 2002;41:313–20.

Ferro BPA, Bouman D. Explanatory notes to the hydrogeological map of Mozambique scale 1:1,000,000. Project of the hydrogeological map of Mozambique. Ministry of Construction and water. National Directorate for water affairs. 1987.

Fournier RO. Chemical geothermometers and mixing models for geothermal systems. Geothermics. 1977;5:41–50.

Fournier RO. Lecture on Geochemical Interpretation of Hydrothermal Waters; UNU Geothermal Training Programme: Reykjavik, Iceland. 1989;10; p. 66

Giggenbach WF. Mass transfer in hydrothermal alterations systems. Geochim Cosmochima Acta. 1984;48:2693–711.

Giggenbach WF, Goguel RL. Collection and analysis of geothermal and volcanic water and gas discharges. Unpublished report, Chemistry Division, DSIR-Petone, New Zealand, 1989. p. 81

Giggenbach WF. Geothermal solute equilibria. Derivation of Na-K-Mg-Ca geoindicators. Geochim Cosmochim Acta. 1988;52:2749–65.

Gleisner M, Herbert RB Jr, Kockum PCF. Pyrite oxidation by Acidithiobacillus ferrooxidans at various concentrations of dissolved oxygen. Chem Geol. 2006;225:16–29.

Groundwater Consultants Bee Pee (Pty) Ltd and SRK Consulting (Pty) Ltd. Compilation of the hydrogeological map atlas: situation analysis Report for the SADC Region. Annex G. 2002.

GTK Consortium. Geology of Degree Sheets Inhamambo, Maluwera, chifunde, Zumbo, Fíngoè-Mâgoè, Songo, Cazula and Zóbuè, Mozambique. Direcção Nacional de Geologia (DNG), Maputo. 2006;4. p.382. sheets 1430–1432 and 1530–1534.

Hankins M. A renewable energy plan for Mozambique. Lori Pottinger; 2009. p. 60.

Hatton W, Fardell A. New Discoveries of coal in Mozambique—development of the coal resource estimation methodology for International Resource Reporting standards. Int J Coal Geol. 2021;89:2–12.

Inguaggiato S, Rizzo A. Dissolved helium isotope ratios in ground waters: a new technique based on gas-water re-equilibration and its application to a volcanic area. Appl Geochem. 2004;19:665–73.

Jennings S, Hasterok D, Lucazeau F. HeatFlow.org: a repository for data and models related to thermal studies of the Earth. 2022. http://heatflow.org/.

Langmuir D. Aqueous environmental geochemistry. Upper Saddle River, NJ: Prentice Hall; 1977. p. 600.

Mamyrin BA, Tolstikhin IN. Helium isotopes in nature. Amsterdam: Elsevier; 1984.

Martinelli G, Dongarrà G, Jones MQW, Rodriguez A. Geothermal features of Mozambique—country update. In: Proceedings of the world geothermal congress, Florence, Italy; 1995. p. 251–261.

Marty B, Jambon A. C/^{3}He in volatile fluxes from the solid earth: implications for carbon geodynamics. Earth Planet Sci Lett. 1987;83:16–26.

Mc Nitt JR. The United Nations approach to geothermal resource assessment. Geothermics. 1978;7:231–42.

Mc Nitt JR. The Geothermal Potential of East Africa. UNESCO/USAD Geothermal Seminar, Nairobi, Kenya; 1982. p. 9

Michard G, Roekens E. Modelling of the chemical composition of alkaline hot waters. Geothermics. 1983;12:161–9.

Michard G. Modification de la répartition des espèces chimiques lors du refroidissement d'une eau thermale. CR Acad Sci. 1977;II(284):949–52.

Minissale A, Vaselli O, Chandrasekharam D, Magro G, Tassi F, Casiglia A. Origin and evolution of "intracratonic" thermal fluids from central-western peninsular India. EPSL. 2000;181:377–94.

Moeck IS. Catalog of geothermal play types based on geologic controls. Renew Sustain Energy Rev. 2014;37:867–82.

Mokveld K, Von Eije S. Final energy report Mozambique, Ministry of Foreign Affairs. 2018.

Mook WG, Bommerson JC, Staverman WH. Carbon isotope fractionation between dissolved carbonate and gaseous carbon dioxide. Earth Planet Sci Lett. 1974;22:169–76.

Moses CO, Herman JS. Pyrite oxidation at circumneutral pH. Geochim Cosmochim Acta. 1991;55:471–82.

Moses CO, Nordstrom DK, Herman JS, Mills AL. Aqueous pyrite oxidation by dissolved oxygen and by ferric iron. Geochim Cosmochim Acta. 1987;51:1561–71.

IRENA. Mozambique, Renewables readiness assessment 2012. pp.73.

Direcçao Nacional de Geologia. Perspectiva sobre os trabalhos de pesquisa preliminar de energia geotermica na RPM, technical report; 1981. p. 6

Nordstrom DK, Plummer LN, Wigley TML, Wolery TJ, Ball JW, Jenne EA, Bassett RL, Crerar DA, Florence TM, Fritz B, Hoffman M, Holdren GR, Lafon GM, Mattigod SV, McDuff RE, Morel F, Reddy MM, Sposito G, Thrailkill J. A comparison of computerized chemical models for equilibrium calculations in aqueous systems. In: Jenne EA editor. Chemical modeling in aqueous systems, ACS symposium series. 1979;93;857–892.

Paquette J, Reeder RJ. Relationship between surface structure, growth mechanism, and trace element incorporation in calcite. Geochim Cosmochim Acta. 1995;9:735–49.

Parkhurst DL, Appelo AAJ. User's guide to PHREEQC (version 2)-a computer program for speciation, batch-reaction, one dimensional transport and inverse geochemical modeling. USGS Water Res Inv Rep. 1999;99:4259.

Pekkala Y, Lehto T, Mäkitie H. GTK consortium geological surveys in Mozambique 2002–2007. Geological Survey of Finland, Special Paper, 2008. p. 321.

Procesi M, Sciarra A, Cinti D, Quattrocchi F, Zarlenga F. Mozambique and the feasible development of the geothermics—a first geochemical survey. WGC, Melbourne, Asutralia; 2015.

Reed M, Spycher N. Calculation of pH and mineral equilibria in hydrothermal waters with application to geothermometry and studies of boiling and dilution. Geochim Cosmochim Acta. 1984;48:1479–92.

Rozanski K, Araguas-Araguas L, Gonfiantini R. Isotope patterns of precipitation in the East African region. In: Johnson T, Odada EO, editors. Limnology, climatology and palaeoclimatology of the east african lakes. Amsterdam: Gordon and Breach Publishers; 1996. p. 79–94.

Schoell M. The hydrogen and carbon isotopic composition of methane from natural gases of various origins. Geochim Cosmochim Acta. 1980;44:649–61.

Steinbruch F, Merkel BJ. Characterization of a Pleistocene thermal spring in Mozambique. Hydrogeol J. 2008;16:1655–68.

Tonani FB, Nagao K, Moore J, Natale G, Sperry T. Water and gas geochemistry of the Cove-Fort Sulphurdale geothermal system. In: Proceedings, twenty-third workshop on geothermal reservoir engineering. Stanford University, Stanford, California; 1998.

Truesdell AH, Fournier RO. Procedure for estimating the temperature of a hot water component in mixed water using a plot of dissolved silica vs. enthalpy. J Res USA Geol Surv. 1977;5:49–52.

United Nations. African hydrogeology, Mozambique. Department of Technical Co-operation for Development. 1989.

Westerhof AB, Tahon A, Koistinen T, Lehto T & Akerman C. Igneous and Tectonic setting of the allochthonous Tete gabbro-anorthosite suite, Mozambique. GTK, Consortium Geological Surveys in Mozambique 2002–2007, vol 48, edited by Geological Survey of Finland. 2008b. p. 191–210.

Westerhof AB, Lehtonen MI, Mäkitie H, Manninen T, Pekkala Y, Gustafsson B & Tahon A. The Tete-Chiapata Belt: a new multiple terrane element from western Momzambique and southern Zambia. GTK, Consortium Geological Surveys in Mozambique 2002–2007, vol 48, edited by Geological Survey of Finland. 2008a. p. 145–166.

Whitfield M. Activity coefficients in natural waters. In: Pytkowicz RM, editor. Activity coefficients in electrolyte solutions. Boca Raton, FL: CRC Press; 1978. p. 153–300.

Williamson MA, Rimstidt JD. Correlation between structure and thermodynamic properties of aqueous sulfur species. Geochim Cosmochim Acta. 1992;56:3867–80.

Williamson MA, Rimstidt JD. The kinetics and electrochemical rate-determining step of aqueous pyrite oxidation. Geochim Cosmochim Acta. 1994;58:5443–54.

Zaporozec A. Graphical interpretation of water-quality data. Ground Water. 1972;10:32–43.

Zhang J, Quay PD, Wilbur DO. Carbon isotope fractionation during gas-water exchange and dissolution of CO_2. Geochim Cosmochim Acta. 1995;82:161–73.

Publisher's Note